

# Cascade Extended State Observer for ADRC Applications under Measurement Noise

Krzysztof Łakomy<sup>a,\*</sup>, Rafał Madonski<sup>b,\*</sup>

<sup>a</sup>*Institute of Automation and Robotics, Poznań University of Technology,  
Piotrowo 3A, 60-965, Poznań, Poland*

<sup>b</sup>*Energy Electricity Research Center, International Energy College, Jinan University,  
Zhuhai, Guangdong, 519070 P. R. China*

---

## Abstract

The extended state observer (ESO) plays an important role in the design of feedback control for nonlinear systems. It is also the key component in any active disturbance rejection control (ADRC) scheme. However, its high-gain nature creates a challenge in engineering practice in cases where the output measurement is corrupted by non-negligible, high-frequency noise. The presence of measurement noise puts a constraint on how high the observer gain can be, which forces a trade-off between fast convergence of state estimates and quality of control task realization. In this brief, a new approach is proposed to redesign the observer part in order to improve its performance in the presence of noise. In particular, a unique cascade combination of ESOs is developed, which is capable of fast and accurate signals reconstruction, while avoiding over-amplification of the measurement noise. The design stage of cascade ESO is followed by the theoretical analysis and the simulation val-

---

\*Corresponding author

*Email addresses:* `krzysztof.lakomy92@gmail.com` (Krzysztof Łakomy),  
`rafal.madonski@jnu.edu.cn` (Rafał Madonski)

idation showing improvement over conventional solution in terms of noise attenuation.

*Keywords:* high-gain observers, noise filtering, active disturbance rejection control, ADRC, extended state observer, ESO

---

## 1. Introduction

A common strategy in the class of active disturbance rejection control (ADRC [1, 2]) techniques for extracting otherwise unavailable information about the governed system is to use an extended state observer (ESO). It simultaneously provides information about the missing state variables (required for controller synthesis) as well as the lumped disturbances/uncertainties (also denoted as *total disturbance* [3]). Successful deployments of ADRC have been well documented in various control areas including process [4], power [5, 6], and motion [7, 8, 9] control.

To a large extent, the performance of any ADRC scheme relies on the speed and accuracy of the ESO [10]. It is well-known that high-gain observers (including ESO) are robust against model uncertainty and disturbances. However, the theory of observers also reveals the existence of a trade-off between speed/accuracy of state reconstruction and sensitivity to high-frequency measurement noise [11]. This problem is still an active research topic with different solutions proposed to date to attenuate the effects of measurement noise. They mainly address the problem by: employing nonlinear ([1, 12]) or adaptive techniques ([13, 14, 15]), redesigning the local behavior by combining different observers ([16, 17, 18, 19]), employing low-power structures ([20, 21]), increasing the observer order with integral

terms [22], adding special saturation functions ([23, 24]), or modifying standard low-pass filters [25, 26].

Motivated by this practically important problem, in this brief, a new paradigm to redesign high-gain observers is proposed in order to improve their performance in the presence of measurement noise. It directly addresses the limitation posed by the trade-off between speed/accuracy of state estimation and noise sensitivity. The principle behind the proposed approach is based on decomposition of the unknown total disturbance into a predefined number of parts, each representing certain signal frequency range, and reconstruction of the decomposed parts with a set of cascaded observers. In contrast to a standard, single-observer ADRC, the introduced multi-observer topology allows to use higher observer bandwidths for reconstructing signals with smaller sensor noise impact. Hence, the contribution of this work is a proposition of the new cascade ESO topology, which is capable of providing fast and accurate estimates while avoiding over-amplification of the sensor noise. To best of our knowledge, such design is presented for the first time in the context of current literature.

*Notation.* Throughout this paper, we use  $\mathbb{R}$  as a set of real numbers,  $\mathbb{R}_+ = \{x \in \mathbb{R} : x > 0\}$  as a set of positive real numbers,  $\mathbb{Z}$  as a set of integers, while  $\mathbf{0}$  and  $\mathbf{I}$  represent zero and identity matrices of the appropriate order, respectively. Relation  $\mathbf{A} \succ 0$  means that  $\mathbf{A}$  is positive-definite,  $\|\mathbf{x}\|$  corresponds to the Euclidean norm of the vector  $\mathbf{x}$ ,  $\|\mathbf{A}\|$  is a matrix norm defined as  $\|\mathbf{A}\| \triangleq \sup\{\|\mathbf{Ax}\| : \mathbf{x} \in \mathbb{R}^n \text{ and } \|\mathbf{x}\| = 1\}$ , while  $\lambda_{\min}(\mathbf{A})$  and  $\lambda_{\max}(\mathbf{A})$  correspond to the minimal and maximal eigenvalues of matrix  $\mathbf{A}$ . Set  $\mathcal{C}^1$  represents a class of locally Lipschitz continuously differentiable functions,

while  $\mathcal{K}$  is a class of strictly increasing functions with the zero-value at the origin.

## 2. Standard ESO design

Before the proposed cascade ESO is explained, theoretically proven, and finally validated in a numerical simulation, let us first recall the standard ESO and highlight its limitations when used in noisy environments. First, a nonlinear dynamical system is represented by the state-space model

$$\begin{cases} \dot{\mathbf{x}}(t) = \mathbf{A}_n \mathbf{x}(t) + \mathbf{b}_n (f(\mathbf{x}, t) + g(\mathbf{x}, t)u(t) + d^*(t)) \\ y(t) = \mathbf{c}_n^\top \mathbf{x}(t) + w(t) \end{cases}, \quad (1)$$

where  $\mathbf{x} \triangleq [x_1 \dots x_n]^\top \in \mathbb{R}^n$  is a system state,  $d^* \in \mathbb{R}$  is an external disturbance,  $u \in \mathbb{R}$  is a control signal,  $y \in \mathbb{R}$  is a system output,  $w \in \mathbb{R}$  corresponds to the measurement noise,  $g \in \mathbb{R}$  describes the influence of the control signal on the system dynamics,  $f \in \mathbb{R}$  represents lumped dynamics of the controlled plant, while  $\mathbf{A}_n \triangleq \begin{bmatrix} \mathbf{0}^{n-1 \times 1} & \mathbf{I}^{n-1 \times n-1} \\ 0 & \mathbf{0}^{1 \times n-1} \end{bmatrix} \in \mathbb{R}^{n \times n}$ ,  $\mathbf{b}_n \triangleq [\mathbf{0}^{n-1 \times 1} \ 1]^\top \in \mathbb{R}^n$ , and  $\mathbf{c}_n \triangleq [1 \ \mathbf{0}^{n-1 \times 1}]^\top \in \mathbb{R}^n$ .

**Assumption 1.** *System (1) is defined on an arbitrarily large bounded domain  $\mathcal{D}_x \subset \mathbb{R}^n$ , such that  $\mathbf{x} \in \mathcal{D}_x$ .*

**Assumption 2.** *Measurement noise is bounded in the sense that there exists a bounded set  $\mathcal{D}_w \subset \mathbb{R}$ , such that  $w \in \mathcal{D}_w$ .*

**Assumption 3.** *External disturbance  $d^*(t) \in \mathcal{C}^1$ , and  $d^* \in \mathcal{D}_{d^*}$ ,  $\dot{d}^* \in \mathcal{D}_{\dot{d}^*}$  for some bounded sets  $\mathcal{D}_{d^*}, \mathcal{D}_{\dot{d}^*} \subset \mathbb{R}$ .*

**Assumption 4.** Fields  $g(\mathbf{x}, t) : \mathcal{D}_x \times \mathbb{R} \rightarrow \mathbb{R}$  and  $f(\mathbf{x}, t) : \mathcal{D}_x \times \mathbb{R} \rightarrow \mathbb{R}$  are continuously differentiable locally Lipschitz functions, i.e.,  $g, f \in \mathcal{C}^1$ .

**Assumption 5.** Utilized control input  $u \in \mathcal{C}^1$ , and  $\sup_{t \geq 0} \{|u(t)|, |\dot{u}(t)|\} < r_u$  for some  $r_u > 0$ .

State dynamics, taken from (1), can be rewritten as

$$\begin{cases} \dot{\mathbf{x}}(t) = \mathbf{A}_n \mathbf{x}(t) + \mathbf{b}_n \hat{g} u(t) \\ \quad + \underbrace{\mathbf{b}_n (f(\mathbf{x}, t) + d^*(t) + (g(\mathbf{x}, t) - \hat{g})u(t))}_{\mathbf{b}_n d(\mathbf{x}, t)} \\ y(t) = \mathbf{c}_n^\top \mathbf{x}(t) + w(t) \end{cases}, \quad (2)$$

where  $d(\mathbf{x}, t) : \mathcal{D}_x \times \mathbb{R} \rightarrow \mathbb{R}$  is the so-called total disturbance, and  $\hat{g} \in \mathbb{R}$  is the rough, constant estimate of  $g$ . Now let us define the extended state  $\mathbf{z} \triangleq [\mathbf{x}^\top d]^\top \in \mathbb{R}^{n+1}$  with the dynamics expressed, according to (2), as

$$\begin{cases} \dot{\mathbf{z}}(t) = \mathbf{A}_{n+1} \mathbf{z}(t) + \mathbf{b}_{n+1} \dot{d}(\mathbf{z}, t) + \mathbf{d}_{n+1} \hat{g} u(t) \\ y(t) = \mathbf{c}_{n+1}^\top \mathbf{z}(t) + w(t) \end{cases}. \quad (3)$$

The standard ESO design, see e.g. [27], is expressed by the dynamics of the extended state estimate  $\hat{\mathbf{z}} := \boldsymbol{\xi}_1 \in \mathbb{R}^{n+1}$ , i.e.,

$$\dot{\boldsymbol{\xi}}_1 = \mathbf{A}_{n+1} \boldsymbol{\xi}_1 + \mathbf{d}_{n+1} \hat{g} u + \mathbf{l}_{1,n+1} (y - \mathbf{c}_{n+1}^\top \boldsymbol{\xi}_1), \quad (4)$$

where  $\mathbf{l}_{1,n+1} \triangleq [\kappa_1 \omega_{o1} \dots \kappa_{n+1} \omega_{o1}^{n+1}]^\top \in \mathbb{R}^{n+1}$  is the observer gain vector dependent on the coefficients  $\kappa_i \in \mathbb{R}_+$  for  $i \in \{1, \dots, n+1\}$  and on the parameter  $\omega_{o1} \in \mathbb{R}_+$ , while  $\mathbf{d}_{n+1} \triangleq [\mathbf{0}^{n-1} \ 1 \ 0]^\top \in \mathbb{R}^{n+1}$ . Observation error can be defined as  $\tilde{\boldsymbol{\xi}}_1 \triangleq \mathbf{z} - \boldsymbol{\xi}_1 \in \mathbb{R}^{n+1}$ , while its dynamics, derived upon (3) and (4), can be

expressed as

$$\dot{\tilde{\boldsymbol{\xi}}}_1 = \underbrace{(\mathbf{A}_{n+1} - \mathbf{l}_{1,n+1}\mathbf{c}_{n+1})}_{\mathbf{H}_1} \dot{\tilde{\boldsymbol{\xi}}}_1 + \mathbf{b}_{n+1}\dot{d} - \mathbf{l}_{1,n+1}w. \quad (5)$$

**Remark 1.** For the sake of notation conciseness of further analysis, we propose to choose the values of  $\kappa_i$  in a way to obtain matrix  $\mathbf{H}_1$  with all eigenvalues equal to  $-\omega_{o1}$ .

**Remark 2.** Under the Assumptions 1-5, the total disturbance  $d \in \mathcal{C}^1$  implying bounded values of its derivative, i.e., guaranteeing  $\dot{d} \in \mathcal{D}_d \subset \mathbb{R}$ . The need to ensure bounded values of  $\dot{d}$ , interpreted as the perturbation of the observation error system (5), is a well-known limitation of the disturbance-observer-based controllers mentioned in [3, 28, 29].

Now, in order to show the influence of total disturbance and measurement noise on the observation errors for standard ESO, let us first introduce a linear change of coordinates  $\tilde{\boldsymbol{\xi}}_1 \triangleq \boldsymbol{\Lambda}_1\boldsymbol{\zeta}_1$ , where  $\boldsymbol{\Lambda}_1 \triangleq \text{diag}\{\omega_{o1}^{-n}, \dots, \omega_{o1}^{-1}, 1\} \in \mathbb{R}^{n+1 \times n+1}$  and  $\boldsymbol{\zeta}_1 \in \mathbb{R}^{n+1}$ , resulting in the transformation of (5) to

$$\begin{aligned} \dot{\boldsymbol{\zeta}}_1 &= \boldsymbol{\Lambda}_1^{-1}\mathbf{H}_1\boldsymbol{\Lambda}_1\boldsymbol{\zeta}_1 + \boldsymbol{\Lambda}_1^{-1}\mathbf{b}_{n+1}\dot{d} - \boldsymbol{\Lambda}_1^{-1}\mathbf{l}_{1,n+1}w \\ &= \omega_{o1}\mathbf{H}^*\boldsymbol{\zeta}_1 + \mathbf{b}_{n+1}\dot{d} - \boldsymbol{\Lambda}_1^{-1}\mathbf{l}_{1,n+1}w, \end{aligned} \quad (6)$$

where

$$\mathbf{H}^* = \begin{bmatrix} -\kappa_1 & 1 & \cdots & 0 \\ \vdots & \vdots & \ddots & \vdots \\ -\kappa_n & 0 & \cdots & 1 \\ -\kappa_{n+1} & 0 & \cdots & 0 \end{bmatrix}. \quad (7)$$

We propose a Lyapunov function candidate  $V_1 = \zeta_1^\top \mathbf{P} \zeta_1$ ,  $V_1 : \mathbb{R}^{n+1} \rightarrow \mathbb{R}$  limited by  $\lambda_{\min}(\mathbf{P}) \|\zeta_1\| \leq V_1 \leq \lambda_{\max}(\mathbf{P}) \|\zeta_1\|$ , where  $\mathbf{P} \succ 0$  is the solution of Lyapunov equation

$$\mathbf{H}^{*\top} \mathbf{P} + \mathbf{P} \mathbf{H}^* = -\mathbf{I}. \quad (8)$$

The derivative of  $V_1$ , derived upon (6), can be expressed as

$$\begin{aligned} \dot{V}_1 &= -\omega_{o1} \zeta_1^\top \zeta_1 + 2\zeta_1^\top \mathbf{P} \mathbf{b}_{n+1} \dot{d} - 2\zeta_1^\top \mathbf{P} \Lambda_1^{-1} \mathbf{l}_{1,n+1} w \\ &\leq -\omega_{o1} \|\zeta_1\|^2 + 2\|\mathbf{P}\| \|\zeta_1\| |\dot{d}| + 2\|\mathbf{P}\| \kappa_{\max} \omega_{o1}^{n+1} w \end{aligned} \quad (9)$$

for  $\kappa_{\max} = \max_j(\kappa_j)$ . The derivative of  $V_1$  holds

$$\begin{aligned} \dot{V}_1 &\leq -\omega_{o1}(1 - \nu_1) \|\zeta_1\|^2 \text{ for} \\ \|\zeta_1\| &\geq \frac{2\|\mathbf{P}\|}{\omega_{o1}\nu_1} |\dot{d}| + \frac{2\|\mathbf{P}\| \kappa_{\max} \omega_{o1}^n}{\nu_1} |w|, \end{aligned} \quad (10)$$

where  $\nu_1 \in (0, 1)$  is a chosen majorization constant and the conservatively estimated lower bound of  $\|\zeta_1\|$  is a class  $\mathcal{K}$  function with respect to arguments  $|\dot{d}|$  and  $|w|$ . According to the result (10), Assumption 2, and Remark 2, we can claim that system (6) is Input-to-State Stable (ISS) with respect to perturbations  $|\dot{d}|$  and  $|w|$ , and referring to Th. 4.19 from [30], satisfies

$$\begin{aligned} \limsup_{t \rightarrow \infty} \|\zeta_1(t)\| &\leq \gamma \frac{2\|\mathbf{P}\|}{\omega_{o1}\nu_1} \sup_{t \geq 0} |\dot{d}(t)| \\ &\quad + \gamma \frac{2\|\mathbf{P}\| \kappa_{\max} \omega_{o1}^n}{\nu_1} \sup_{t \geq 0} |w(t)| \\ &\leq \gamma \frac{2\|\mathbf{P}\|}{\omega_{o1}\nu_1} r_d + \gamma \frac{2\|\mathbf{P}\| \kappa_{\max} \omega_{o1}^n}{\nu_1} r_w \end{aligned} \quad (11)$$

for  $\gamma = \sqrt{\lambda_{\max}(\mathbf{P})/\lambda_{\min}(\mathbf{P})}$ ,  $\{|\dot{d}| < r_d\} \subset \mathcal{D}_d$ , and  $\{|w| < r_w\} \subset \mathcal{D}_w$ . To achieve the minimal asymptotic upper-bound of the transformed observation

error  $\|\zeta_1\|$ , we need to find a trade-off between the reduction of  $|\dot{d}|$  impact with the increasing  $\omega_{o1}$  values and the influence of  $|w|$  amplified by  $\omega_{o1}^n$ . It is worth noting, that for the nominal case when  $\dot{d}(t) \equiv 0$  and  $w(t) \equiv 0$ , the asymptotic upper bound of  $\limsup_{t \rightarrow \infty} \|\zeta_1\| = 0$ , implying the asymptotic upper bound of the original observation error vector  $\limsup_{t \rightarrow \infty} \|\tilde{\xi}_1\| = 0$ . In the case of non-zero values of  $|\dot{d}|$  and  $w(t) \equiv 0$ ,  $\|\zeta_1\| \rightarrow 0$  as  $\omega_{o1} \rightarrow \infty$  and  $t \rightarrow \infty$ .

**Remark 3.** *Since in the practical conditions the value of parameter  $\omega_{o1} \gg 1$ , inequality  $\|\tilde{\xi}_1\| \leq \lambda_{max}(\Lambda_1) \|\zeta_1\|$  implies that the asymptotic relation (11) and all of the further comments hold also for the original observation error  $\|\tilde{\xi}_1\|$ .*

### 3. Cascade ESO: concept

The concept of ADRC relies on the feedforward cancellation of the total disturbance included in the generic controller

$$u = \hat{g}^{-1}(-\hat{d} + v), \quad (12)$$

where  $v$  represents the new virtual control signal, most commonly in the form of a stabilizing feedback controller.

Substitution of (12) into the dynamics (2) results in the closed-loop form of the considered system described by

$$\dot{\mathbf{x}} = \mathbf{A}_n \mathbf{x} + \mathbf{b}_n \tilde{d} + \mathbf{b}_n v, \quad (13)$$

where  $\tilde{d} = d - \hat{d} \in \mathbb{R}$  is the residual total disturbance. Let us now assume that the parameter  $\omega_{o1}$  of the standard ESO, see (4), was set to a relatively low value which only allows a precise following of the first element of extended

state, i.e.  $\mathbf{c}_{n+1}^\top \mathbf{z}$ , but filters out the measurement noise  $w(t)$ . Latter elements of the extended state are dependent on the further derivatives of the first one, and usually are more dynamic and have faster transients, thus are not estimated precisely by ESO using chosen  $\omega_{o1}$ . As a consequence, values of the total disturbance residue  $\tilde{d}$  can be substantial causing a possible loss of control precision.

To improve the estimation performance of the extended state obtained with the standard ESO with low  $\omega_{o1}$ , treated here as a first level in the cascade observer structure, let us introduce the state vector of the second level of the observer  $\boldsymbol{\xi}_2 \triangleq [\hat{\xi}_{1,1} \ \widehat{\xi_{1,1}^{(1)}} \ \dots \ \widehat{\xi_{1,1}^{(n-1)}} \ \hat{d}]^\top \in \mathbb{R}^{n+1}$ , where  $\widehat{\xi_{1,1}^{(i)}}$  for  $i \in \{1, \dots, n-1\}$  is the estimate of  $i$ -th derivative of  $\xi_{1,1}$ , while  $\hat{d}$  represents estimated value of a residual total disturbance. The structure of second observer level is designed as

$$\begin{aligned} \dot{\boldsymbol{\xi}}_2(t) &= \mathbf{A}_{n+1} \boldsymbol{\xi}_2(t) + \mathbf{d}_{n+1} v(t) + \mathbf{l}_{2,n+1} \mathbf{c}_{n+1}^\top (\boldsymbol{\xi}_1(t) - \boldsymbol{\xi}_2(t)) \\ &\stackrel{(12)}{=} \mathbf{A}_{n+1} \boldsymbol{\xi}_2(t) + \mathbf{d}_{n+1} (\hat{g}u(t) + \mathbf{b}_{n+1}^\top \boldsymbol{\xi}_1(t)) \\ &\quad + \mathbf{l}_{2,n+1} \mathbf{c}_{n+1}^\top (\boldsymbol{\xi}_1(t) - \boldsymbol{\xi}_2(t)) \end{aligned} \quad (14)$$

where  $\mathbf{l}_{2,n+1} \triangleq [\kappa_1 \omega_{o2} \ \dots \ \kappa_{n+1} \omega_{o2}^{n+1}]^\top \in \mathbb{R}^{n+1}$  and  $\omega_{o2} = \alpha \omega_{o1}$ ,  $\alpha > 1$ . Note that the equation of the second observer level does not depend on the system output  $y$ , thus is not affected by the measurement noise directly. The estimate of total disturbance utilized in (12) should be now taken from the new extended state estimate

$$\hat{\mathbf{z}} := \boldsymbol{\xi}_2 + \mathbf{b}_{n+1} \mathbf{b}_{n+1}^\top \boldsymbol{\xi}_1 \quad (15)$$

A block diagram of the ADRC control structure with the proposed cascade ESO (for  $p = 2$ ) applied to the system (1) is shown in Fig. 1.

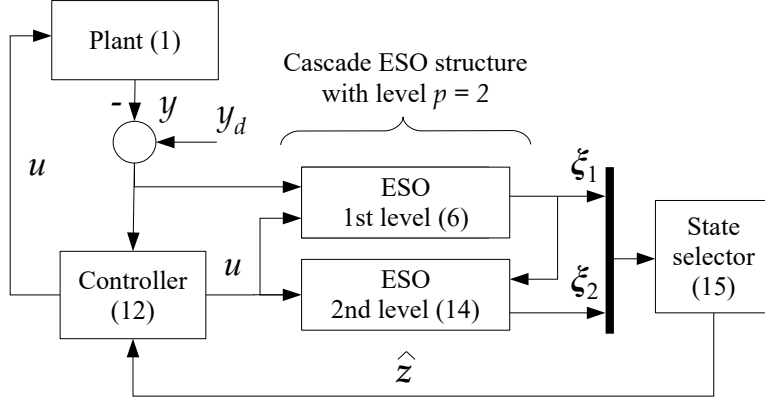


Figure 1: Block diagram of an ADRC structure including proposed cascade ESO for  $p = 2$ .

**Remark 4.** *Coefficients  $\kappa_i$  of cascade observer can differ in general between the cascade levels, but for the sake of notation clarity, we assume within this article that they are equal.*

**Remark 5.** *The idea of the cascade observer topology is to estimate the total disturbance observation residue resulting from the previous level with the next cascade level of ESO, implying that the observer bandwidth multiplier  $\alpha > 1$*

The observation error, associated with the cascade observer with two levels, can be defined as

$$\tilde{\xi}_2 = z - \xi_2 - \mathbf{b}_{n+1} \mathbf{b}_{n+1}^\top \xi_1, \quad (16)$$

with its dynamics derived upon (14), (4), and (3) as

$$\dot{\tilde{\xi}}_2 = \mathbf{H}_2 \tilde{\xi}_2 + \mathbf{\Gamma}_{2,1} \tilde{\xi}_1 + \delta_2 w + \mathbf{b}_{n+1} \dot{d} \quad (17)$$

for  $\mathbf{H}_2 = \mathbf{A}_{n+1} - \mathbf{l}_{2,n+1} \mathbf{c}_{n+1}^\top$ ,  $\mathbf{\Gamma}_{2,1} = \mathbf{l}_{2,n+1} \mathbf{c}_{n+1}^\top - \mathbf{b}_{n+1} \mathbf{b}_{n+1}^\top \mathbf{l}_{1,n+1} \mathbf{c}_{n+1}^\top$  and  $\delta_2 = -\mathbf{b}_{n+1} \mathbf{b}_{n+1}^\top \mathbf{l}_{1,n+1}$ .

Following the reasoning presented in Sect. 2 for standard ESO, we now prove that the observation error  $\tilde{\boldsymbol{\xi}}_2$  is bounded, despite a perturbing impact of total disturbance and measurement noise. Let us introduce a linear change of coordinates  $\tilde{\boldsymbol{\xi}}_2 \triangleq \boldsymbol{\Lambda}_2 \boldsymbol{\zeta}_2$  for  $\boldsymbol{\Lambda}_2 \triangleq \text{diag}\{\omega_{o2}^{-n}, \dots, \omega_{o2}^{-1}, 1\} \in \mathbb{R}^{n+1 \times n+1}$ , and  $\boldsymbol{\zeta}_2 \in \mathbb{R}^{n+1}$ . The dynamics of  $\boldsymbol{\zeta}_2$  is described by

$$\begin{aligned} \dot{\boldsymbol{\zeta}}_2 &= \boldsymbol{\Lambda}_2^{-1} \mathbf{H}_2 \boldsymbol{\Lambda}_2 \boldsymbol{\zeta}_2 + \boldsymbol{\Lambda}_2^{-1} \boldsymbol{\Gamma}_{2,1} \boldsymbol{\Lambda}_1 \boldsymbol{\zeta}_1 + \boldsymbol{\Lambda}_2^{-1} \boldsymbol{\delta}_2 w + \boldsymbol{\Lambda}_2^{-1} \mathbf{b}_{n+1} \dot{d} \\ &= \omega_{o2} \mathbf{H}^* \boldsymbol{\zeta}_2 + \boldsymbol{\Lambda}_2^{-1} \boldsymbol{\Gamma}_{2,1} \boldsymbol{\Lambda}_1 \boldsymbol{\zeta}_1 + \boldsymbol{\Lambda}_2^{-1} \boldsymbol{\delta}_2 w + \mathbf{b}_{n+1} \dot{d} \end{aligned} \quad (18)$$

for matrix  $\mathbf{H}^*$  taken from (7). Let us introduce a Lyapunov function candidate in the form  $V_2 \triangleq \boldsymbol{\zeta}_2^\top \mathbf{P} \boldsymbol{\zeta}_2$ ,  $V_2 : \mathbb{R}^{n+1} \rightarrow \mathbb{R}$  limited by  $\lambda_{\min}(\mathbf{P}) \|\boldsymbol{\zeta}_2\| \leq V_2 \leq \lambda_{\max}(\mathbf{P}) \|\boldsymbol{\zeta}_2\|$ , where  $\mathbf{P}$  is a solution of the Lyapunov equation (8). The derivative of  $V_2$ , calculated with (18), has the form

$$\begin{aligned} \dot{V}_2 &= -\omega_{o2} \boldsymbol{\zeta}_2^\top \boldsymbol{\zeta}_2 + 2\boldsymbol{\zeta}_2^\top \mathbf{P} \boldsymbol{\Lambda}_2^{-1} \boldsymbol{\Gamma}_{2,1} \boldsymbol{\Lambda}_1 \boldsymbol{\zeta}_1 + 2\boldsymbol{\zeta}_2^\top \mathbf{P} \boldsymbol{\Lambda}_2^{-1} \boldsymbol{\delta}_2 w \\ &\quad + 2\boldsymbol{\zeta}_2^\top \mathbf{P} \mathbf{b}_{n+1} \dot{d} \\ &\leq -\omega_{o2} \|\boldsymbol{\zeta}_2\|^2 + 2\kappa_{\max} \alpha^{n+1} \omega_{o1} \|\mathbf{P}\| \|\boldsymbol{\zeta}_1\| \|\boldsymbol{\zeta}_2\| \\ &\quad + 2\kappa_{\max} \omega_{o1}^{n+1} \|\mathbf{P}\| |w| \|\boldsymbol{\zeta}_2\| + 2 \|\mathbf{P}\| |\dot{d}| \|\boldsymbol{\zeta}_2\|, \end{aligned} \quad (19)$$

which holds

$$\begin{aligned} \dot{V}_2 &\leq -\omega_{o2}(1 - \nu_2) \|\boldsymbol{\zeta}_2\|^2 \text{ for} \\ \|\boldsymbol{\zeta}_2\| &\geq \frac{2\kappa_{\max} \alpha^n \|\mathbf{P}\|}{\nu_2} \|\boldsymbol{\zeta}_1\| + \frac{2\kappa_{\max} \omega_{o1}^n \|\mathbf{P}\|}{\alpha \nu_2} |w| + \frac{2 \|\mathbf{P}\|}{\omega_{o2} \nu_2} |\dot{d}|, \end{aligned} \quad (20)$$

where  $\nu_2 \in (0, 1)$  is a chosen majorization constant and the conservatively estimated lower bound of the transformed observation error  $\|\boldsymbol{\zeta}_2\|$  is a class  $\mathcal{K}$  function with respect to the arguments  $\|\boldsymbol{\zeta}_1\|$ ,  $|w|$ , and  $|\dot{d}|$ . According to

the result (20), the system (18) is ISS and satisfies the asymptotic relation

$$\begin{aligned}
\limsup_{t \rightarrow 0} \|\zeta_2(t)\| &\leq \gamma \frac{2\kappa_{\max} \alpha^n \|\mathbf{P}\|}{\nu_2} \limsup_{t \rightarrow \infty} \|\zeta_1(t)\| \\
&+ \gamma \frac{2\kappa_{\max} \omega_{o1}^n \|\mathbf{P}\|}{\alpha \nu_2} \sup_{t \geq 0} |w(t)| + \frac{2 \|\mathbf{P}\|}{\omega_{o2} \nu_2} \sup_{t \geq 0} |\dot{d}(t)| \\
&\stackrel{(11)}{\leq} \gamma \left[ \frac{2\kappa_{\max} \omega_{o1}^n \|\mathbf{P}\|}{\alpha \nu_2} + \frac{4\kappa_{\max}^2 \alpha^n \omega_{o1}^n \|\mathbf{P}\|^2}{\nu_2 \nu_1} \right] r_w \\
&+ \gamma \left[ \frac{2 \|\mathbf{P}\|}{\omega_{o2} \nu_2} + \frac{4\kappa_{\max} \alpha^n \|\mathbf{P}\|^2}{\nu_2 \nu_1 \omega_{o1}} \right] r_d, \tag{21}
\end{aligned}$$

for  $\gamma$ ,  $r_d$ ,  $r_w$  having the same values as the ones from (11). Summarizing, the transformed observation error is bounded in general,  $\|\zeta_2\| \rightarrow 0$  as  $\omega_{o1} \rightarrow \infty$  and  $t \rightarrow \infty$  when  $w \equiv 0$ , and  $\limsup_{t \rightarrow \infty} \|\zeta_2(t)\| = 0$  when both  $w \equiv 0$  and  $\dot{d} \equiv 0$ . Similarly to the issue described in Remark 3 for the single-stage observer, the original observation error for the second-level cascade observer ( $p = 2$ ) satisfies  $\|\tilde{\xi}_2\| \leq \lambda_{\max}(\mathbf{\Lambda}_2) \|\zeta_2\| = \max\left\{\frac{1}{\omega_{o2}^n}, 1\right\} \|\zeta_2\|$ , and thus holds the ISS property itself.

#### 4. Cascade ESO: general design

In the general case, we may continue the procedure of estimating residual observation errors by increasing the level of observer cascade to the arbitrarily chosen value  $p = k$  such that  $k \in \mathbb{Z}$  and  $k \geq 2$ . The cascade observer with  $i$  levels can be written down as

$$\begin{aligned}
\dot{\xi}_1(t) &= \mathbf{A}_{n+1} \xi_1(t) + \mathbf{d}_{n+1} \hat{g}u(t) + \mathbf{l}_{1,n+1} (y(t) - \mathbf{c}_{n+1}^\top \xi_1(t)) \\
\dot{\xi}_i(t) &= \mathbf{A}_{n+1} \xi_i(t) + \mathbf{d}_{n+1} \left( \hat{g}u(t) + \mathbf{b}_{n+1}^\top \sum_{j=1}^{i-1} \xi_j(t) \right) \\
&+ \mathbf{l}_{i,n+1} \mathbf{c}_{n+1}^\top (\xi_{i-1}(t) - \xi_i(t)) \tag{22}
\end{aligned}$$

for  $i \in \{2, \dots, p\}$  and  $\omega_{oi} = \alpha \omega_{oi-1}$  for  $\alpha > 1$ . The estimate of total disturbance implemented in (12) can be taken from the new extended state estimate expressed as

$$\hat{z} := \xi_i + \mathbf{b}_{n+1} \mathbf{b}_{n+1}^\top \sum_{j=1}^{i-1} \xi_j. \quad (23)$$

A block diagram of the ADRC control structure with the proposed cascade ESO (in its general form  $p = k$ ) for the system (1) is shown in Fig. 2.

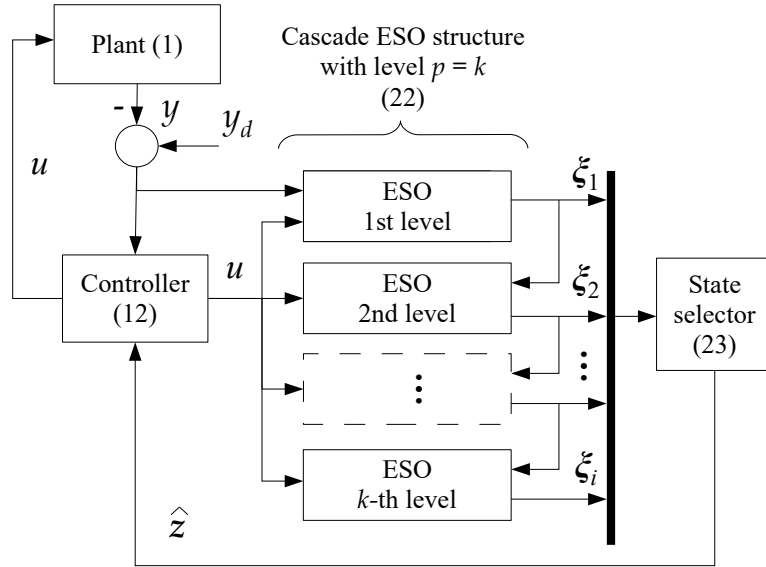


Figure 2: Block diagram of an ADRC structure including proposed cascade ESO for  $p = k$ .

The observation error for the  $i$ -level cascade ESO

$$\tilde{\xi}_i \triangleq z - \xi_i - \mathbf{b}_{n+1} \mathbf{b}_{n+1}^\top \sum_{j=1}^{i-1} \xi_j \quad (24)$$

with the dynamics expressed (after some algebraic manipulations made ac-

ording to (3), and (22)) as

$$\dot{\tilde{\boldsymbol{\xi}}}_i = \mathbf{H}_i \tilde{\boldsymbol{\xi}}_i + \boldsymbol{\Gamma}_{i,i-1} \tilde{\boldsymbol{\xi}}_{i-1} + \mathbf{b}_{n+1}^\top \dot{d} + \sum_{j=1}^{i-2} \boldsymbol{\Gamma}_{i,j} \tilde{\boldsymbol{\xi}}_j + \boldsymbol{\delta}_i w \quad (25)$$

for  $\mathbf{H}_i = \mathbf{A}_{n+1} - \mathbf{l}_{i,n+1} \mathbf{c}_{n+1}^\top$ ,  $\boldsymbol{\Gamma}_{i,i-1} = \mathbf{l}_{i,n+1} \mathbf{c}_{n+1}^\top - \mathbf{b}_{n+1} \mathbf{b}_{n+1}^\top \mathbf{l}_{i-1,n+1} \mathbf{c}_{n+1}^\top$ ,  $\boldsymbol{\Gamma}_{i,j} = -\mathbf{b}_{n+1} \mathbf{b}_{n+1}^\top \mathbf{l}_{j,n+1} \mathbf{c}_{n+1}^\top$ , and  $\boldsymbol{\delta}_i = -\mathbf{b}_{n+1} \mathbf{b}_{n+1}^\top \mathbf{l}_{1,n+1}$ . Using the linear change of coordinates  $\boldsymbol{\xi}_i = \boldsymbol{\Lambda}_i \boldsymbol{\zeta}_i$  for  $\boldsymbol{\Lambda}_i \triangleq \text{diag}\{-\omega_{o1}^{-n}, \dots, -\omega_{o1}^{-1}, 1\} \in \mathbb{R}^{n+1 \times n+1}$  and  $\boldsymbol{\zeta}_i \in \mathbb{R}^{n+1}$ , we may rewrite the observation error dynamics concerning  $i$ -th level structure as

$$\begin{aligned} \dot{\boldsymbol{\zeta}}_i &= \underbrace{\boldsymbol{\Lambda}_i^{-1} \mathbf{H}_i \boldsymbol{\Lambda}_i}_{\omega_{oi} \mathbf{H}^*} \boldsymbol{\zeta}_i + \boldsymbol{\Lambda}_i^{-1} \boldsymbol{\Gamma}_{i,i-1} \boldsymbol{\Lambda}_{i-1} \boldsymbol{\zeta}_{i-1} + \boldsymbol{\Lambda}_i^{-1} \mathbf{b}_{n+1} \dot{d} \\ &\quad + \boldsymbol{\Lambda}_i^{-1} \sum_{j=1}^{i-2} \boldsymbol{\Gamma}_{i,j} \boldsymbol{\Lambda}_j \boldsymbol{\zeta}_j + \boldsymbol{\Lambda}_i^{-1} \boldsymbol{\delta}_i w. \end{aligned} \quad (26)$$

To prove the boundedness of observation errors in the general case of cascade ESO, let us propose a Lyapunov function candidate defined as  $V_i \triangleq \boldsymbol{\zeta}_i^\top \mathbf{P} \boldsymbol{\zeta}_i$ ,  $V_i : \mathbb{R}^{n+1} \rightarrow \mathbb{R}$  and bounded by  $\lambda_{\min}(\mathbf{P}) \|\boldsymbol{\zeta}_2\| \leq V_2 \leq \lambda_{\max}(\mathbf{P}) \|\boldsymbol{\zeta}_2\|$ , where  $\mathbf{P}$  is a solution of an algebraic Lyapunov equation (8). The derivative of  $V_i$  is calculated upon (26) and takes the form

$$\begin{aligned} \dot{V}_i &= -\omega_{oi} \boldsymbol{\zeta}_i^\top \boldsymbol{\zeta}_i + 2\boldsymbol{\zeta}_i^\top \mathbf{P} \boldsymbol{\Lambda}_i^{-1} \boldsymbol{\delta}_i w + 2\boldsymbol{\zeta}_i^\top \mathbf{P} \boldsymbol{\Lambda}_i^{-1} \mathbf{b}_{n+1} \dot{d} \\ &\quad + 2\boldsymbol{\zeta}_i^\top \mathbf{P} \boldsymbol{\Lambda}_i^{-1} \boldsymbol{\Gamma}_{i,i-1} \boldsymbol{\Lambda}_{i-1} \boldsymbol{\zeta}_{i-1} + 2\boldsymbol{\zeta}_i^\top \mathbf{P} \boldsymbol{\Lambda}_i^{-1} \sum_{j=1}^{i-2} \boldsymbol{\Gamma}_{i,j} \boldsymbol{\Lambda}_j \boldsymbol{\zeta}_j \\ &\leq -\omega_{oi} \|\boldsymbol{\zeta}_i\|^2 + 2 \|\mathbf{P}\| \|\boldsymbol{\zeta}_i\| \kappa_{\max} \omega_{o1}^{n+1} |w| + 2 \|\mathbf{P}\| \|\boldsymbol{\zeta}_i\| |\dot{d}| \\ &\quad + 2 \frac{\kappa_{\max} \omega_{oi}^{n+1}}{\omega_{oi-1}^n} \|\mathbf{P}\| \|\boldsymbol{\zeta}_{i-1}\| \|\boldsymbol{\zeta}_i\| + 2 \|\mathbf{P}\| \|\boldsymbol{\zeta}_i\| \sum_{j=1}^{i-2} \omega_{oj} \|\boldsymbol{\zeta}_j\| \end{aligned} \quad (27)$$

that holds

$$\begin{aligned}
\dot{V}_i &\leq -\omega_{oi}(1 - \nu_i) \|\zeta_i\|^2 \text{ for} \\
\|\zeta_i\| &\geq \frac{2\kappa_{\max}\omega_{oi}^n \|\mathbf{P}\|}{\nu_i\omega_{oi}^n} \|\zeta_{i-1}\| \\
&+ \frac{2\|\mathbf{P}\|}{\nu_i\omega_{oi}} \sum_{j=1}^{i-2} \omega_{oj} \|\zeta_j\| + \frac{2\|\mathbf{P}\|}{\nu_i\omega_{oi}} |\dot{d}| + \frac{2\|\mathbf{P}\| \kappa_{\max}\omega_{o1}^{n+1}}{\nu_i\omega_{oi}} |w| \\
&= \frac{2\kappa_{\max}\alpha^n \|\mathbf{P}\|}{\nu_i} \|\zeta_{i-1}\| + \frac{2\|\mathbf{P}\|}{\nu_i} \sum_{j=1}^{i-2} \frac{1}{\alpha^{i-j}} \|\zeta_j\| \\
&+ \frac{2\|\mathbf{P}\|}{\nu_i\alpha^{i-1}\omega_{o1}} |\dot{d}| + \frac{2\|\mathbf{P}\| \kappa_{\max}\omega_{o1}^n}{\nu_i\alpha^{i-1}} |w|. \tag{28}
\end{aligned}$$

According to the ISS procedure, steady-state values of the transformed observation error are limited by

$$\begin{aligned}
\limsup_{t \rightarrow \infty} \|\zeta_i(t)\| &\leq \gamma \frac{2\kappa_{\max}\alpha^n \|\mathbf{P}\|}{\nu_i} \limsup_{t \rightarrow \infty} \|\zeta_{i-1}(t)\| \\
&+ \gamma \frac{2\|\mathbf{P}\|}{\nu_i} \sum_{j=1}^{i-2} \frac{1}{\alpha^{i-j}} \limsup_{t \rightarrow \infty} \|\zeta_j(t)\| \\
&+ \gamma \frac{2\|\mathbf{P}\|}{\nu_i\alpha^{i-1}\omega_{o1}} \sup_{t \geq 0} |\dot{d}(t)| + \gamma \frac{2\|\mathbf{P}\| \kappa_{\max}\omega_{o1}^{n-1}}{\nu_i\alpha^{i-1}} \sup_{t \geq 0} |w(t)|, \tag{29}
\end{aligned}$$

where  $\gamma$  is taken from (11). Due to the recursive character of the obtained asymptotic relation and the result (11), we may also write that  $\limsup_{t \rightarrow \infty} \|\zeta_i\| \leq c_1 r_{\dot{d}} + c_2 r_w$  for some positive constants  $c_1, c_2$  dependent on the parameters  $\omega_{o1}$  and  $\alpha$ . As it was presented for previously described observer structures, transformed observation error is generally bounded,  $\|\zeta_i\| \rightarrow 0$  as  $\omega_{o1} \rightarrow \infty$  and  $t \rightarrow \infty$  when  $w(t) \equiv 0$ , and  $\limsup_{t \rightarrow \infty} \|\zeta_i(t)\| = 0$  when both  $w(t) \equiv 0$  and  $\dot{d}(t) \equiv 0$ . Similarly to the issue described in Remark 3 for the single-level observer structure, the original observation error for the  $i$ -level cascade

observer  $\|\tilde{\boldsymbol{\xi}}_i\| \leq \lambda_{\max}(\mathbf{\Lambda}_i) \|\boldsymbol{\zeta}_i\| = \max\left\{\frac{1}{\omega_{oi}^n}, 1\right\} \|\boldsymbol{\zeta}_i\|$  and thus holds the ISS property itself.

## 5. Numerical verification

### 5.1. Methodology

In order to evaluate the effectiveness of the proposed cascade ESO-based ADRC design (Sect. 3 and 4) in terms of control objective realization and measurement noise attenuation, its results are quantitatively compared with the results from a standard, single ESO-based ADRC design (Sect. 2). For the purpose of this case study, a following second order system in form of (1) is considered:

$$\begin{cases} \dot{\mathbf{x}}(t) = \mathbf{A}_2 \mathbf{x}(t) + \mathbf{b}_2(f(\mathbf{x}) + g \cdot u(t) + d^*(t)) \\ y(t) = \mathbf{c}_2^\top \mathbf{x}(t) + w(t) \end{cases}, \quad (30)$$

with  $\mathbf{x} = \begin{bmatrix} x_1 \\ x_2 \end{bmatrix}$ ,  $f(\mathbf{x}) = -x_1 - 2x_2$ , and  $g = 1$ . The core linear dynamics of (30) is affected (starting at  $t = 3.5\text{s}$ ) by an external, nonlinear disturbance  $d^*(t) = 5 \sin(9t)$ . The control objective is to make the output  $y(t)$  track a desired trajectory  $y_d(t) \in \mathbb{R}$  in the presence of measurement noise  $w(t)$  and despite the influence of  $d^*(t)$ . Signal  $y_d(t)$  here is a step function, additionally filtered by a stable dynamics  $G_f(s) = 1/(0.1s + 1)^5$  to minimize the observer peaking. The control action  $u$  is defined the same for all tested cases as in (12), with  $v = \ddot{y}_d + 4(\dot{y}_d - \xi_{p,2}) + 4(y_d - \xi_{p,1})$ . To keep the conciseness of notation, we treat the standard ESO as the case with  $p = 1$ . Two comparison tests are performed.

*SimA: trajectory tracking without measurement noise.* In order to establish a fair base for further comparison in the presence of measurement noise, similar performance between the tested control designs is achieved first in the idealized, noise-less conditions ( $w(t) = 0$ ). Since total disturbance estimation is the key element in any ADRC approach, the focus here is on providing similar reconstruction quality of  $\hat{d}$  in terms of minimizing integral criterion  $\int |\tilde{z}_3(t)|dt$ , with  $\tilde{z}_3(t)$  being the total disturbance observation error taken from  $\tilde{\mathbf{z}} = [\tilde{z}_1 \ \tilde{z}_2 \ \tilde{z}_3]^\top \triangleq \tilde{\boldsymbol{\xi}}_p$ . Since the tested control algorithms do not share similar observer structure, nor have the same number of tuning parameters, it is arbitrarily decided to use a tuning methodology of single observer bandwidth parameterization from [27], which is based on a standard pole-placement procedure (cf. *Remark 1*). The heuristically selected observer bandwidths from Table 1 provide the similar total disturbance reconstruction quality among the tested algorithms, as confirmed by Table 2. Two integral criteria are additionally introduced to evaluate overall tracking accuracy ( $10^3 \int |e(t)|dt$ ) and energy usage ( $\int |u(t)|dt$ ), with  $e(t) \triangleq y_d(t) - y(t)$  being the feedback error.

*SimB: trajectory tracking with measurement noise.* This time, a more realistic scenario is considered in which the output measurement noise is present (i.e.  $w(t) \neq 0$ ), hence the only change w.r.t. test *SimA* is the introduction of the band-limited white noise  $w(t)$  with power  $1e^{-10}$ .

## 5.2. Results and discussion

The results of *SimA* are gathered in Fig. 3. The selected observer bandwidths provide visually comparable results of total disturbance estimation er-

Table 1: Control designs used in the comparison.

Observer type	Observer bandwidth
Standard ESO $p=1$	$\omega_{o1} = 400$
Proposed ESO $p=2$	$\omega_{o1} = 75, \omega_{o2} = 2\omega_{o1}$
Proposed ESO $p=3$	$\omega_{o1} = 40, \omega_{o2} = 2\omega_{o1}, \omega_{o3} = 2\omega_{o2}$

Table 2: Assessment based on selected integral quality criteria.

Test	Observer type	Criterion		
		$10^3 \int  e(t) dt$	$\int  u(t) dt$	$\int  \tilde{z}_3(t) dt$
<i>SimA</i>	Standard ESO $p=1$	9.963	46.949	<b>0.521</b>
	Proposed ESO $p=2$	6.297	50.096	<b>0.520</b>
	Proposed ESO $p=3$	4.355	49.013	<b>0.521</b>
<i>SimB</i>	Standard ESO $p=1$	10.031	98.922	10.092
	Proposed ESO $p=2$	6.615	53.563	3.120
	Proposed ESO $p=3$	4.625	51.540	2.881

ror ( $\tilde{z}_3(t)$ ) and energy consumption ( $u(t)$ ) in all tested control designs, even though both cascade ESO-based designs have significantly lower observer bandwidths than standard approach. The proposed cascade ESO structures also improve the tracking quality ( $e(t)$ ) despite having lower observer bandwidths. The observation error  $\tilde{z}_1(t)$  differs among tested techniques noticeably, however, it is expected result since in the cascade observer design, the importance of output signal estimation is being shifted and favors total disturbance estimation instead. It is done deliberately and has practical justification as it is often the case that the output signal is available directly through measurement, hence its close estimation would be redundant.

The results of *SimB* are gathered in Fig. 4. The cascade ESO provides improvement in noise attenuation over standard ESO, especially in the quality of total disturbance reconstruction and, consequently, in the control signal profile (Table 2). With the extra layer of cascade ( $p = 3$ ), the amplitude of noise is further reduced. It is not surprising since with the increase of cascade level, lower observer bandwidths can be selected for estimating signals contaminated with high-frequency noise (hence noise is not over-amplified). At the same time, high observer bandwidths can be selected for estimating signals which are affected by the noise to a smaller extent, hence high tracking capabilities can be retained.

Additionally, Fig. 5 shows relative quality of total disturbance estimation (understood as minimizing criterion  $\int |\tilde{z}_3(t)|dt$ ) between standard and proposed ESO-based designs in tests *SimA* (left) and *SimB* (right). The blue color represents area where the total disturbance is estimated more precisely with ESO associated with the horizontal axis, while the red color represents

the area where an ESO structure related to the vertical axis provides better estimation. The dashed lines in the left-hand side figures connect points with equal values of estimation precision, i.e., cases having similar convergence speed of observation error. Black dots placed on each plot are representing the parameter values utilized in the simulations illustrated in time-domain in Fig. 3 and Fig. 4. When the same dashed line is plotted in the right-hand side figure associated with the comparison of standard ESO and the proposed one (both for  $p = 2$  and  $p = 3$ ), it is surrounded by blue area for high observer bandwidths ( $\omega_{o1}$ ) of standard ESO. This confirms numerically that the use of cascade ESO is justified when high observer gains are demanded, as it can improve the estimation precision (connected with noise attenuation) for similar convergence speed. The comparison of cascaded ESO structures for  $p = 2$  and  $p = 3$  shows that in the presence of measurement noise, the estimation quality is (a) equal for both structures, when the dashed line lays on the border of blue and red area, (b) better for  $p = 2$  level structure for a small range of relatively low values of  $\omega_{o1}$  when the dashed line is on the red area, and (c) more precise for  $p = 3$  level cascade ESO in the case of dashed line laying on the blue area. However, case with  $p = 3$  revealed (expectedly) that there is a limit to the cascade level increase. And although it is shown through the obtained numerical results that the introduction of cascade ESO structure can be beneficial in sensor noise suppression, both the specific value of  $p$  and the ESO gains should be tailored on a case-by-case basis. General methodology for  $p$  selection and observer tuning is still an open question.

## 6. Conclusions

From the obtained results, one can deduce that the compromise between speed/accuracy of state reconstruction and noise amplification is still present, however, with the cascade ESO one gains extra degree of freedom in designing high-bandwidth observers while minimizing the amplification of output noise. This reveals great practical potential of the proposed method in high-performance control of systems subjected to non-negligible measurement noise. The potential drawbacks of the proposed cascade ESO-based design (like extra tuning parameters, lack of a systematic method of cascade level selection and cascade ESO tuning) need to be further investigated. Future work includes comprehensive comparison (both quantitative and qualitative) with other noise attenuation techniques dedicated to high-gain observers (see Introduction) as well as experimental validation.

## References

- [1] J. Han, From PID to Active Disturbance Rejection Control, *IEEE Transactions on Industrial Electronics* 56 (3) (2009) 900–906.
- [2] Z. Gao, On the centrality of disturbance rejection in automatic control, *ISA Transactions* 53 (4) (2014) 850–857.
- [3] S. Chen, Z. Chen, On active disturbance rejection control for a class of uncertain systems with measurement uncertainty (early access), *IEEE Transactions on Industrial Electronics* (2020) 1–1.
- [4] Z. Wu, D. Li, Y. Xue, L. Sun, T. He, S. Zheng, Modified active dis-

- turbance rejection control for fluidized bed combustor (in press), ISA Transactions.
- [5] L. Sun, Q. Hua, D. Li, L. Pan, Y. Xue, K. Y. Lee, Direct energy balance based active disturbance rejection control for coal-fired power plant, ISA Transactions 70 (2017) 486–493.
  - [6] L. Dong, Y. Zhang, Z. Gao, A robust decentralized load frequency controller for interconnected power systems, ISA Transactions 51 (3) (2012) 410–419.
  - [7] R. Patelski, P. Dutkiewicz, On the stability of adrc for manipulators with modelling uncertainties (in press), ISA Transactions.
  - [8] M. M. Michałek, K. Łakomy, W. Adamski, Robust output-feedback cascaded tracking controller for spatial motion of anisotropically-actuated vehicles, Aerospace Science and Technology 92 (2019) 915 – 929.
  - [9] R. Madonski, M. Kordasz, P. Sauer, Application of a disturbance-rejection controller for robotic-enhanced limb rehabilitation trainings, ISA Transactions 53 (4) (2014) 899–908.
  - [10] R. Madonski, P. Herman, Survey on methods of increasing the efficiency of extended state disturbance observers, ISA Transactions 56 (2015) 18–27.
  - [11] H. K. Khalil, L. Praly, High-gain observers in nonlinear feedback control, International Journal of Robust and Nonlinear Control 24 (6) (2014) 993–1015.

- [12] A. A. Prasov, H. K. Khalil, A nonlinear high-gain observer for systems with measurement noise in a feedback control framework, *IEEE Transactions on Automatic Control* 58 (3) (2013) 569–580.
- [13] J. H. Ahrens, H. K. Khalil, High-gain observers in the presence of measurement noise: a switched-gain approach, *Automatica* 45 (4) (2009) 936–943.
- [14] R. G. Sanfelice, L. Praly, On the performance of high-gain observers with gain adaptation under measurement noise, *Automatica* 47 (10) (2011) 2165–2176.
- [15] S. Battilotti, Robust observer design under measurement noise with gain adaptation and saturated estimates, *Automatica* 81 (2017) 75–86.
- [16] N. Boizot, E. Buswelle, J. P. Gauthier, An adaptive high-gain observer for nonlinear systems, *Automatica* 46 (2010) 1483–1488.
- [17] D. Astolfi, R. Postoyan, D. Nesic, Uniting local and global observers for the state estimation of nonlinear continuous-time systems, in: *Proc. Conference on Decision and Control*, 2017, pp. 3039–3044.
- [18] A. Zemouche, F. Zhang, F. Mazenc, R. Rajamani, High-gain nonlinear observer with lower tuning parameter, *IEEE Transactions on Automatic Control* 64 (8) (2019) 3194–3209.
- [19] W. Xue, X. Zhang, L. Sun, H. Fang, Extended state filter based disturbance and uncertainty mitigation for nonlinear uncertain systems with application to fuel cell temperature control (early access), *IEEE Transactions on Industrial Electronics* (2020) 1–1.

- [20] L. Wang, D. Astolfi, L. Marconi, H. Su, High-gain observers with limited gain power for systems with observability canonical form, *Automatica* 75 (2017) 16–23.
- [21] H. K. Khalil, Cascade high-gain observers in output feedback control, *Automatica* 80 (2017) 110–118.
- [22] K. K. Busawon, P. Kabore, Disturbance attenuation using proportional integral observers, *International Journal of Control* 74 (6) (2001) 618–627.
- [23] L. Z. D. Astolfi, A. Alessandri, Stubborn ISS redesign for nonlinear high-gain observers, in: *Proc. IFAC World Congress*, 2017.
- [24] G. Herbst, Practical active disturbance rejection control: bumpless transfer, rate limitation, and incremental algorithm, *IEEE Transactions on Industrial Electronics* 63 (3) (2016) 1754–1762.
- [25] D. Astolfi, M. Jungers, L. Zaccarian, Output injection filtering redesign in high-gain observers, in: *Proc. European Control Conference*, 2018, pp. 1957–1962.
- [26] H. K. Khalil, S. Priess, Analysis of the use of low-pass filters with high-gain observers, *IFAC-PapersOnLine* 49 (18) (2016) 488–492, *IFAC Symposium on Nonlinear Control Systems*.
- [27] Z. Gao, Scaling and bandwidth-parameterization based controller tuning, in: *Proc. American Control Conference*, Vol. 6, 2003, pp. 4989–4996.

- [28] D. Astolfi, L. Marconi, A high-gain nonlinear observer with limited gain power, *IEEE Transactions on Automatic Control* 60 (11) (2015) 3059–3064.
- [29] W. Xue, Y. Huang, Performance analysis of active disturbance rejection tracking control for a class of uncertain LTI systems, *ISA Transactions* 58 (2015) 133–154.
- [30] H. K. Khalil, *Nonlinear systems*, 3rd edition, Prentice Hall, New Jersey, 2002.

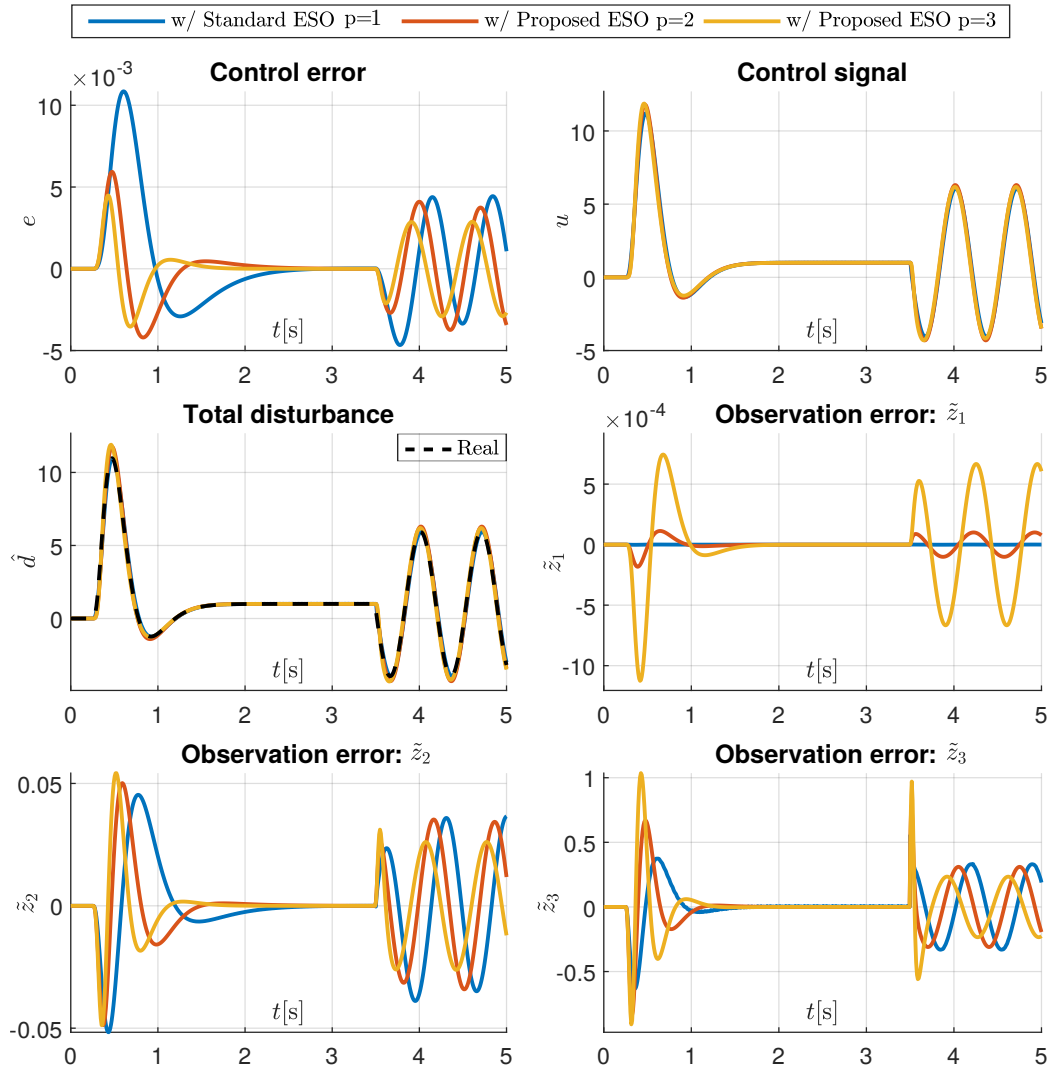


Figure 3: Results of test *SimA* (i.e. without measurement noise:  $w(t) = 0$ ).

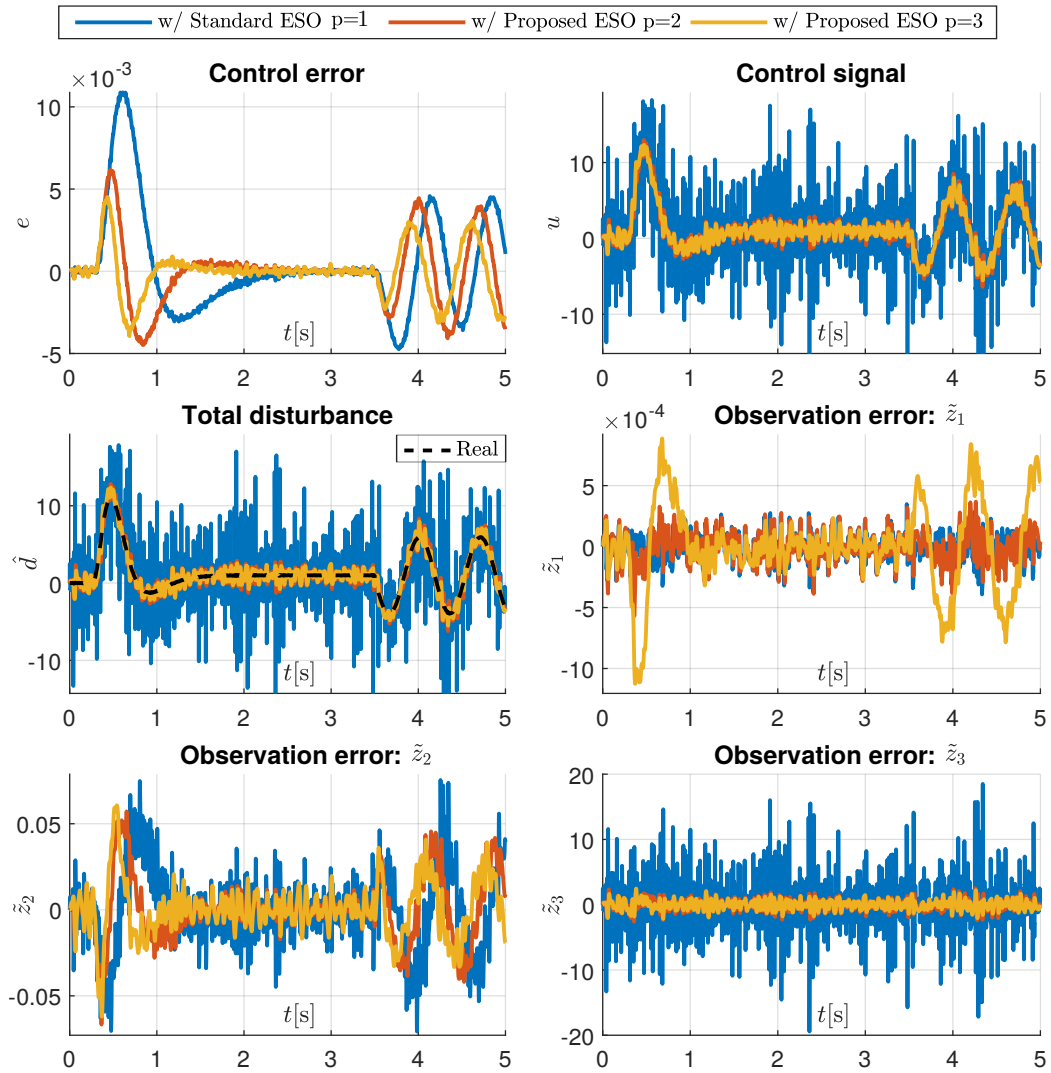


Figure 4: Results of test *SimB* (i.e. with measurement noise:  $w(t) \neq 0$ ).

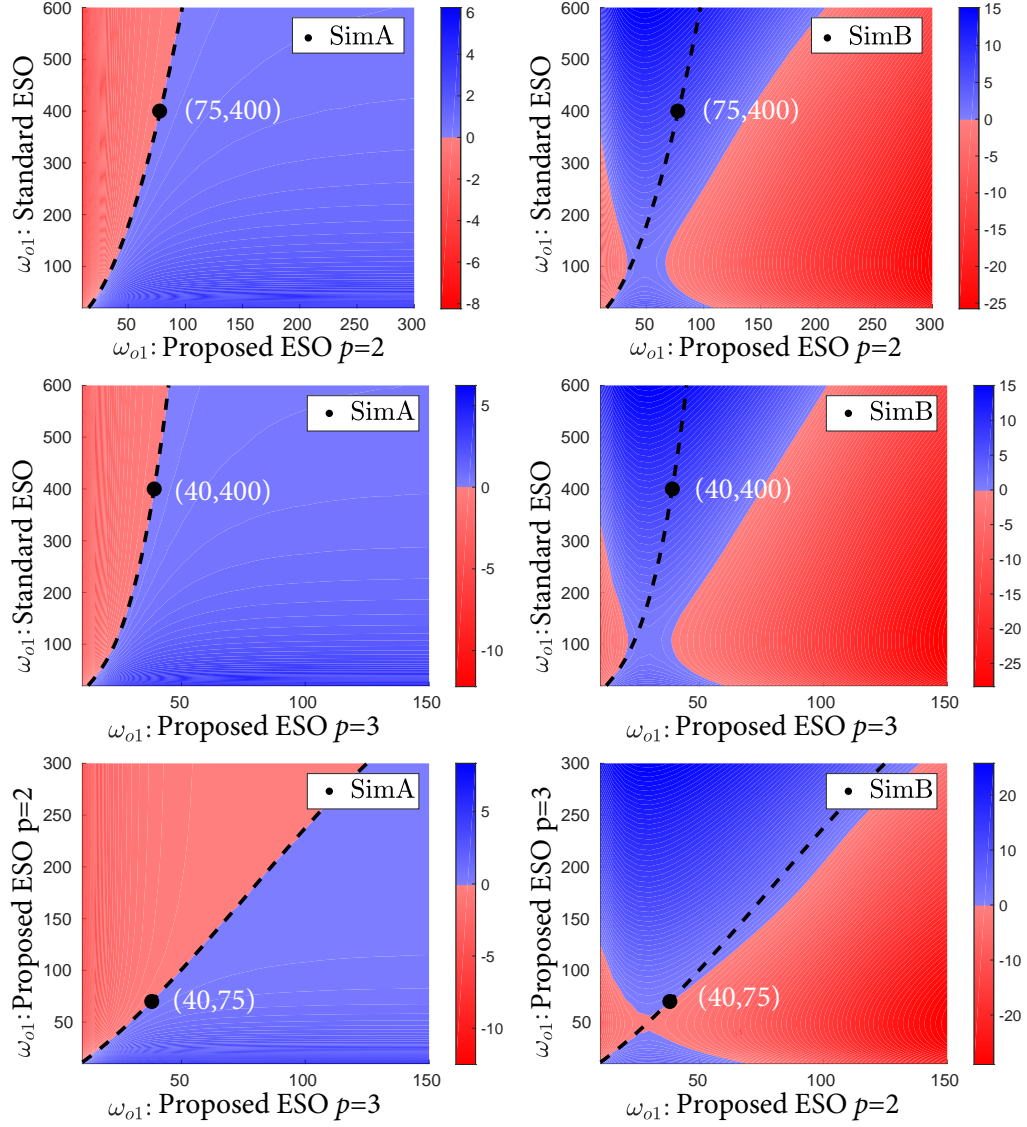


Figure 5: Difference between  $\int |\tilde{z}_3(t)| dt$  values obtained for the standard and the proposed ESOs ( $p = 2$  and  $p = 3$ ). Left-hand side figures are related to the simulations without measurement noise ( $w(t) = 0$ ), while the figures on the right-hand side are associated with the cases where the measurement noise is present ( $w(t) \neq 0$ ). Black dots represent the specific pair of observer bandwidths used in both tests (see Table 1).